ELSEVIER

Bone Vol. 20, No. 5
May 1997:485–490

Determining Mineral Content Variations in Bone Using Backscattered Electron Imaging

R. D. BLOEBAUM,[1] J. G. SKEDROS,[1] E. G. VAJDA,[1] K. N. BACHUS,[2] and B. R. CONSTANTZ[3]

[1] *Bone and Joint Research Laboratory, Veterans Affairs Medical Center, Salt Lake City, UT, USA*
[2] *Orthopaedic Bioengineering Research Laboratory, Department of Orthopedics, University of Utah, Salt Lake City, UT, USA*
[3] *Norian Corporation, Cupertino, CA, USA*

The mechanical properties of bones are greatly influenced by the ratio of organic constituents to mineral. Determination of bone mineral content on a macroscopic scale is straightforward, but microscopic variations, which can yield new insights into remodelling activities, mechanical strength, and integrity, are profoundly more difficult to measure. Measurement of microscopic mineral content variations in bone material has traditionally been performed using microradiography. Backscattered electron (BSE) imaging is a technique with significantly better resolution than microradiography with demonstrated consistency, and it does not suffer from projection-effect errors. We report results demonstrating the applicability of quantitative BSE imaging as a tool for measuring microscopic mineral content variations in bones representing a broad range of mineralization. Bones from ten species were analyzed with Fourier-transformed infrared spectroscopy, X-ray diffraction, energy dispersive X-ray spectrometry, ash measurements, and BSE imaging. BSE image intensity (graylevel) had a very strong positive correlation to mineral (ash) content. Compositional and crystallographic variations among bones had negligible influence on backscattered electron graylevels. The present study confirms the use of BSE imaging as a tool to measure the microscopic mineral variability in a broad range of mineralized tissues. (Bone 20:485–490; 1997)

Key Words: Backscattered electron imaging; Bone density; Ash fraction; Mineral content; Microscopic; Calcified tissue.

Introduction

The measurement of mineral content in bones and mineralized tissue at the macroscopic level is of great interest to biologists and zoologists. Bone mineral content can be viewed in two contexts, as described by Martin and Burr.[27] Volumetric mineralization is a measure of the amount of mineral per unit volume of whole bone, and is therefore influenced both by mineral content and porosity of the bone. Specific mineralization, however, is a measure of the amount of mineral per unit volume of bone tissue (excluding porosity). This study addresses the measurement of specific mineralization.

Address for correspondence and reprints: R. D. Bloebaum, Bone and Joint Research Laboratory, VA Medical Center (151F), 500 Foothill Boulevard, Salt Lake City, UT 84148.

It is well established that small adjustments in specific mineral content can significantly affect the mechanical properties of bone.[12,14,15] In nature, there are conspicuous examples of some bones that have adapted their relative mineral content to accommodate specific mechanical loading conditions. For example, deer antler is low-mineral-content bone, making it ductile with a large work of fracture.[13] This accommodates the impact loading conditions that antlers of most deer species must endure during the mating season. In contrast, the whale tympanic bulla is very highly mineralized, an adaptation that is not for mechanical loading, but for acoustic impedance.[13]

Microscopic variations in a bone's mineral content, although difficult to measure, may explain much of the variation in its mechanical properties, particularly in pathological mineralized tissue. Microradiography was developed as a technology to evaluate microscopic mineral content variations in thin sections of bones and other mineralized tissues.[1,28,35,41] However, the utility of microradiography is limited by resolution. The highest resolution of microradiographs of bone has been estimated[23,35] to represent a cylindrical volume on the order of 400–4000 μm^3. Errors caused by projection effects[2,42] can further limit the accuracy and use of microradiography in histometric and mineral content analyses. Additionally, studies requiring the microradiographic analysis of relatively large numbers of specimens can be difficult to accomplish because all specimens must be ground or milled to a uniform thickness (typically 100 μm) and calibration between laboratories has yet to be documented.

To circumvent these problems, backscattered electron (BSE) imaging in the scanning electron microscope (SEM) was developed as a tool for determining qualitative differences in the mineralization of bone and dental tissues.[7,8,10] Depending on SEM operating conditions, Howell and Boyde[23] estimated that the volumetric resolution of BSE images in bone ranged from 0.07 to 137 μm^3, which is considerably better than the highest resolution in microradiography. This is probably an underestimation of the resolution because Howell and Boyde incorrectly calculated the atomic number of bone using a simple mean, rather than a weighted mean.[25,33,39] If Howell and Boyde[23] had estimated the atomic number of hydroxyapatite to be 14.1 rather than 11.4, then the resolution would be even greater.[23,39] Due to the improved resolution, BSE imaging technology has been extensively used for qualitative analysis,[7,8,10,18,21] but has only recently been developed into a rigorous, calibrated, quantitative method[5,6,9,31,33,38,39,43,44] of mineral content analysis with experimentally demonstrated consistency.[5,33,44]

The use of BSE imaging to determine mineral content is based on the well-established principle that the fraction of

8756-3282/97/$17.00
PII S8756-3282(97)00015-X

Bone Vol. 20, No. 5
May 1997:485–490

Table 1. List of bone specimens and their anatomical provenances

Species		Anatomical location
Human (S162)	*Homo sapiens*	midshaft, anterior cortex, femur
Human (S141)	*Homo sapiens*	midshaft, anterior cortex, femur
Cow	*Bos taurus*	midshaft, anterior cortex, femur
Fin whale	*Balaenoptera physalus*	tympanic bulla
Rocky Mountain mule deer	*Odocoileus hemionus hemionus*	proximal shaft, cranial cortex, calcaneus
Rocky Mountain mule deer	*Odocoileus hemionus hemionus*	antler
King penguin	*Aptenodytes patagonica*	midshaft, cortex, humerus
Sheep	*Ovis aries*	midshaft, anterior cortex, tibia
Greyhound dog (D282)	*Canis familiaris*	midshaft, anterior cortex, femur
Greyhound dog (D56)	*Canis familiaris*	midshaft, anterior cortex, femur
Greyhound dog (D85)	*Canis familiaris*	midshaft, medial cortex, tibia
Rabbit	*Lepus sp.*	midshaft, cortex, femur
Semiaquatic turtle	*Chelydra serpentina*	midshaft, cortex, tibia
White leghorn chicken	*Gallus domesticus*	diaphysis, whole femur, embryo

[a]Numbers in parentheses after human and dog specimens are accession numbers used to distinguish specimens. The two human and three dog specimens were obtained from five different donors.

electrons that collide with a target sample and then travel to a detector as backscattered electrons, increases monotonically as a function of the average atomic number of the sample.[22] The resulting BSE signal can be converted into a digital black/white image where the intensity (graylevel) of any pixel in the image is proportional to the mean atomic number of the corresponding location on the target material. Some investigators have suggested that the BSE signal, therefore, represents the mineral density of bone.[7,9,31,43] This interpretation may be incorrect because experimental evidence reveals that the BSE signal is not proportional to density in pure elements.[4] Other investigators have demonstrated that graylevels in calibrated BSE images of simulated bone tissues have a strong positive correlation with both mineral content and density.[38] Similar results have been observed in bones obtained from chickens ranging in age from embryo to adult.[39] However, these early studies measured volume percent mineral (vol. mineral/vol. total), and, as Roschger et al.[33] suggested on theoretical grounds, the use of weight percent mineral (wt. mineral/wt. total) would be preferable. Nevertheless, a strong linear relationship was observed in these earlier studies, and is undoubtedly the result of the strong positive correlations among density, weight percent mineral, and volume percent mineral.[39] These correlations have not yet been validated in bone tissues from various species over a broad range of mineralization. Additionally, the effect that variations in composition and crystallography have on the BSE signal in bones has not been adequately assessed. Small variations in the composition of the mineral phase of bone, which have been observed between species,[3] may alter BSE image graylevels. Mineral crystallite size and orientation may also play a role in BSE image graylevels. The objectives of this study are to: (1) quantitatively demonstrate that BSE images graylevels in bone are linearly correlated to ash fraction over a broad range of species with a broad range of mineralization; and (2) demonstrate that compositional and crystallographic variations have minimal influence on BSE graylevels.

Materials and Methods

Specimen Preparation

Bones selected for this study were obtained from various anatomical locations in ten species (**Table 1**). Each bone was cut into five adjacent segments. One segment from each bone was used for BSE image graylevel analysis. Two segments from each bone were used for ash percent measurements. The remaining two segments from each bone were used for compositional and crystallographic analyses. The embryonic chick femur was too small to be sectioned into five individual segments, and therefore compositional and crystallographic analyses were conducted on the femora from age-matched chicks. All five segments from each bone were defatted in a large volume of reagent grade chloroform, dried in an oven at 80°C for 5 days, and weighed on an analytical balance. Volume of all five segments from each bone was measured using a helium micropycnometer.[45] Bone density was calculated from the volume and weight measurements of each segment.

BSE Analysis

Specimens that were analyzed in the BSE mode of the SEM were embedded in polymethyl methacrylate,[17,36,37] cut into cubes with a band saw, and glued together with a cyanoacrylate glue. The composite specimen block was ground and polished with 0.5-μm alumina to an optical finish, and lightly sputter-coated with gold. The composite specimen block was placed on the stage of a Jeol 6100 SEM (Jeol USA, Inc., Peabody, MA) equipped with a Tetra (Oxford Instruments, Cambridge, UK) solid-state BSE detector, with the polished surface perpendicular to the incident electron beam. SEM operating conditions included: 30-kV accelerating voltage; 15-mm working distance; 0.75-nA probe current; and images were captured in the BSE mode with nine scans using a Kalman frame averaging technique. SEM operating conditions were stored in computer memory and restored prior to every image capture. Probe current was measured with a SM-16100 probe current detector (Jeol) attached to an external picoammeter (Keithley Instruments, Cleveland, OH) prior to every image capture and manually adjusted by fine alterations of the condenser lens strength as necessary. Five BSE images were collected from each embedded bone segment at 200×. BSE images were collected as 512 × 512 pixel, digital images with 256 distinct graylevels. The weighted mean graylevel (WMGL) of each image was calculated following the equation previously described[4,44]:

$$\mathrm{WMGL} = \sum_{i=6}^{255} \frac{A_i \mathrm{GL}_i}{A_t}$$

where: A_i = area of ith graylevel; GL_i = ith graylevel; and A_t = total area imaged. This provides a mean value for the backscat-

tered signal, independent of porosity (black pixels 0–5 in the BSE image). To ensure instrument stability, BSE-image WMGLs were calibrated at 20-min intervals using a magnesium alloy (99.8% pure; 93% Mg, 6% Al, and 1% Zn; Johnson Matthey, Inc., Seabrook, NH) and pure aluminum (99.9999% pure, Johnson Matthey) as calibration standards following the protocol of Vajda et al.[44] A mechanized stage was utilized to ensure that the same microscopic regions of the calibration standards were analyzed throughout the course of the experiment. Quantitative, experimental studies have demonstrated the applicability of this technique.[5,44]

Ash Measurements

Bone segments used for ash percent measurements were defatted and dried, as described previously, and placed in an oven at 550°C for 24 h to remove organic constituents. The weight of the specimens was determined before and after ashing using a precision analytical balance. Ash percent is expressed as ashed bone weight (W_{AB}) divided by dry, defatted bone weight (W_{DB}) multiplied by 100 [$(W_{AB}/W_{DB})*100$].

Compositional Analysis

Compositional and crystallographic analyses consisted of Fourier-transformed infrared spectroscopy (FTIR), energy dispersive X-ray spectrometry (EDX), and X-ray diffraction (XRD). FTIR samples were ground with a mortar and pestle, and FTIR spectroscopy was performed on 1-mg samples pressed in 300 mg KBr pellets with a Nicolet 5DXC FTIR spectrometer.

EDX measurements were performed on a Jeol 6100 SEM equipped with a beryllium window X-ray detector (Pentafet, Oxford Instruments). Measurements were performed on the same composite specimen block used for BSE analysis. Operating conditions included an accelerating voltage of 20.0 kV, working distance of 15 mm, probe current of 2.50 nA, and a live capture time of 130 sec. Pure $CaCO_3$ and InP were used as reference standards for ZAF corrections.[20] ZAF corrections were performed using the ZAF-4 software program (eXL Image Analysis System, Oxford Instruments). EDX measurements were used to obtain Ca/P molar ratios.

Powder X-ray diffraction measurements using Cu $K\alpha$ radiation were performed on samples ground with a mortar and pestle, packed in stainless-steel sample holders, and scanned with a Scintag TTGON10 θ-θ goniometer. XRD samples were analyzed from 4° to 35° 2θ with a step size of 2θ/step. Counting time was set at 20 sec/step. Bone samples were qualitatively compared with a pure sintered hydroxyapatite standard (Calcitek Calcitite 4060-2, Lot #892436, Norian Corp., Cupertino, CA). Scherrer crystal sizes[11] were calculated using the 002 peak near 26° 2θ. The Scherrer formula provides an estimate of the average perfect crystallite size in one dimension, based on XRD peak widths. FTIR and XRD analyses were performed by the Norian Corporation.

Results

Density and ash percent measurements (**Table 2**) demonstrate broad variability among the species. Visual inspection of BSE images revealed conspicuous graylevel differences among the species (**Figure 1**). Low-mineral-content tissues appeared much darker than high-mineral-content tissues. Morphological features, lamellar patterns, and graylevel differences were observed within individual images. Pearson correlation demonstrated that ash percent was very strongly correlated ($r^2 = 0.937$; $p < 0.000001$) to WMGL (**Figure 2**). A moderate positive correlation ($r^2 = 0.622$; $p < 0.001$) was also observed between density and WMGL (Figure 2). Both ash percent and density correlations dramatically improve if the data excludes the embryonic chick femur, which appears to be an outlier ($r^2 = 0.973$ and $r^2 = 0.858$, respectively; Figure 2).

Table 2. Density data (g/cm^3), ash percent data (%), weighted mean graylevel (WMGL) data (graylevels), calcium-to-phosphorus (Ca/P) molar ratios (mol/mol), and Scherrer crystal size calculations (Å)

Species	Density	Ash percent	WMGL	Ca/P	Scherrer
Human (S162)	2.11	70.7	109.9	1.66	203
Human (S141)	2.13	70.1	107.6	1.72	203
Cow	2.12	73.5	127.0	1.62	172
Fin whale	2.49	85.8	172.2	1.61	190
Mule deer calcaneus	2.06	71.4	109.5	1.61	190
Mule deer antler	1.89	61.6	57.7	1.55	143
King penguin	2.21	74.7	125.3	1.63	172
Sheep	2.17	74.4	125.3	1.66	190
Greyhound dog (D282)	2.20	72.2	111.5	1.63	203
Greyhound dog (D56)	2.13	73.4	123.5	1.65	203
Greyhound dog (D85)	2.11	70.5	104.0	1.62	172
Rabbit	2.34	75.4	136.6	1.62	163
Semiaquatic turtle	2.10	68.3	96.9	1.84	136
White leghorn chicken	0.77	52.1	53.4	1.71	NA

NA = not available.

FTIR showed all samples to be comprised of a carbonated apatite. No significant variation in the composition of the mineral phase was observed among specimens. EDX measurements of weight percent calcium and phosphorous were used to calculate Ca/P molar ratios, which confirmed compositional similarity among the specimens (Table 2). No correlation ($r^2 = 0.030$; $p > 0.5$) between Ca/P molar ratios and WMGL was observed. X-ray diffraction data demonstrated that all specimens were poorly crystalline carbonated apatites. Perfect Scherrer crystal size estimates (Table 2) ranged from 136 Å (turtle) to 203 Å (human and dog). No significant correlation between Scherrer size and WMGL was found with a Pearson correlation ($r^2 = 0.170$; $p > 0.1$). The XRD spectra obtained from the embryonic chick femur were masked by noise and it was not possible to reliably calculate the Scherrer crystal size. The embryonic chick femur was therefore not included in the Pearson correlation.

Discussion

The high positive correlation between ash percent and WMGL over a broad range of mineralized tissue demonstrates that mineral content can be reliably determined from graylevel analysis of BSE images. Similarly, density was strongly correlated to WMGL, with the exclusion of the embryonic chick femur, which supports the conceptual model of bone mineralization, as described by Richelle and Onkelinx.[32] Their model predicts that, during normal bone mineralization, progressive increases in mineral content are primarily the result of progressive increases in the packing density of mineral crystals in and on the collagen framework. Therefore, a higher mineral content would be expected to coincide with increased density. However, the strength of the correlation coefficients was not equal. A stronger correlation was observed between BSE graylevels and mineral content than between BSE graylevels and density, supporting Roschger and co-workers'[33] suggestion that future investigators should interpret BSE-image graylevels as proportional to weight percent mineral.

The most noticeable deviation from these correlations is the

Bone Vol. 20, No. 5
May 1997:485–490

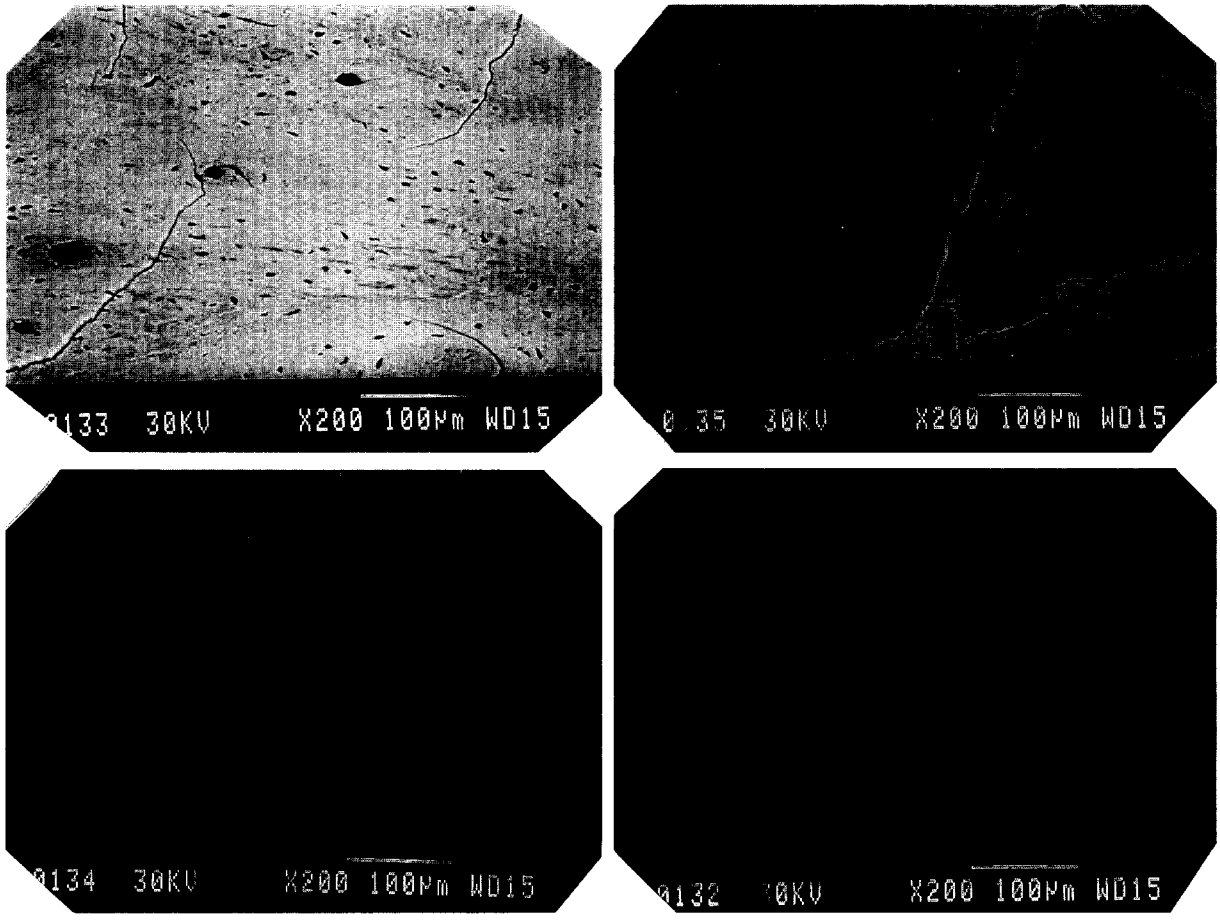

Figure 1. Backscattered electron photomicrographs of four specimens with varied mineral content. In all four images, morphological features are clearly visible. The images are arranged in order of decreasing overall graylevel (mineral content): (a) fin whale tympanic bulla; (b) rabbit femur; (c) human femur; and (d) Rocky Mountain mule deer antler. Brightness and contrast have been set to allow visualization of all specimens in one imaging session. Optimal visual appearance for any individual species, which would have a smaller range of mineral content values, could be improved by increasing contrast. Cracks in the specimens are unavoidable artifacts of preparation. Similarly, the bright border surrounding the cracks cannot be interpreted as regions of highly mineralized tissue. Rather, they are artifacts due to electron interactions near the crack surface.

embryonic chick femur, which has a lower mineral content and lower density than would be expected from the correlation data. The embryonic chick skeleton is typically composed of rapidly forming bone with substantial pore volume.[30] Therefore, manual removal of marrow and soft tissues is considerably more difficult than in the other bones. The relatively rapid renewal of bone tissue in the embryonic stage,[19] compared with the other bone specimens which are from mature animals, would also result in a larger residual amount of unmineralized bone (osteoid) in the embryonic chick. With the SEM contrast and brightness settings used in this study, osteoid and soft tissue that had not been completely removed from the chick femur would appear black in a BSE image, making it indistinguishable from the polymethyl methacrylate embedding media. Failure to adequately remove soft tissues and infiltrate the pores with polymethyl methacrylate would therefore not be expected to dramatically affect the WMGL. The presence of these soft tissues would, however, artificially *increase* the dry, defatted bone weight which would *decrease* ash percent (mineral content) and density, accounting for the deviations from the regression line.

FTIR and EDX data demonstrate that all of the tissues involved in this study have similar mineral composition. Small quantities of brushite, whitlockite, and other minerals have been reported to occur in bone in previous studies,[16,24,34] but were not observed in this study. Small compositional variations in the mineral phase, if present in this study, are so small (<1% by weight) that they are beyond the detection limits of the FTIR and EDX analysis methods and hence are not likely to explain the large variations in graylevel intensity observed in the BSE images.

XRD data demonstrate that all of the specimens in the study were relatively microcrystalline. Published data confirm that the range of crystallite size estimates in this study are of an order of magnitude comparable to other bones in previous studies.[26] Comparison with XRD data from a sintered hydroxyapatite standard shows that even the most ordered of the bone specimens in this study (fin whale tympanic bulla) is far less structured than pure, sintered, stoichiometric hydroxyapatite, indicating relatively poor crystallinity. The lack of correlation between Scherrer crystal size and WMGL suggests that average crystal size and order in bone has minimal influence on BSE image graylevels.

This study demonstrates that it is not only possible to measure variations in the mineralization of bone at the macroscopic level, which is of great interest with respect to mechanical properties, but it is possible to use BSE imaging technology to measure mineral variations at the microscopic level without disrupting the underlying morphology. The coefficient of determination (r^2) of

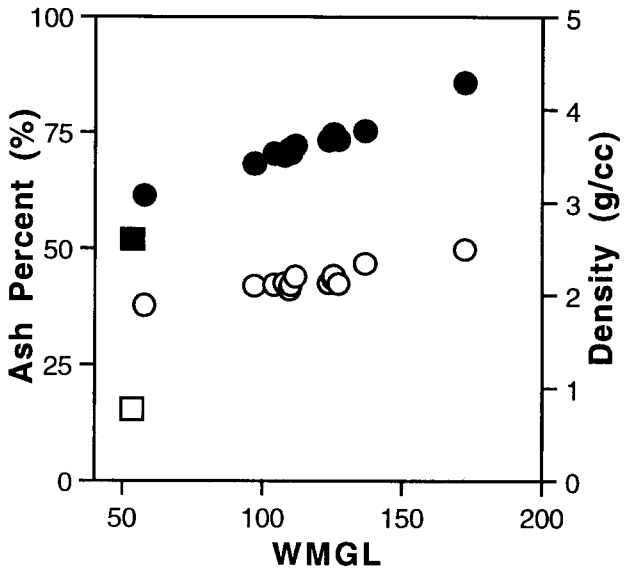

Figure 2. Scatterplot between backscattered electron image weighted mean graylevel (WMGL) and ash percent demonstrating a high positive correlation (solid symbols; $r^2 = 0.937$). Scatterplot between WMGL and density shows a moderate positive correlation (open symbols; $r^2 = 0.622$). The embryonic chick femur (squares) appears at the low end of the WMGL scale and is an apparent outlier. Correlations dramatically increase with the exclusion of the embryonic chick femur ($r^2 = 0.973$ and $r^2 = 0.858$ for ash and density, respectively).

0.973 signifies that greater than 97% of the variation in WMGL of tissues examined in the present study can be attributed to mineral content variations. The lamellar patterns and anomalous graylevel values seen near cracks cannot, however, be interpreted solely as mineral content variations. Other investigators have suggested that the lamellar patterns are the result of topographical fluctuations and can be eliminated by diamond micromilling specimens,[8,23] rather than the conventional grinding and polishing used in the present study. Examination of published photomicrographs of micromilled specimens[8,33,40] reveals that lamellar contrast may be reduced, but it is not eliminated. The lamellar patterns may be the result of both surface topography and mineral content variation, and the relative contribution of the two factors is unknown. This calls into question the ultimate resolution at which BSE graylevels can be correlated to ash content. In studies that seek to examine mineral differences in extremely small regions (e.g., between two individual lamellae) topographical relief must be considered a potential complicating factor. Theoretical calculations of the relative importance of topography have been previously addressed,[23] and experimental investigations are currently being conducted in our laboratory. Nonetheless, the present study experimentally demonstrates that BSE graylevels obtained from microscopic regions of bone are highly correlated to mineral content. The contribution of topographical relief to the BSE signal in the current study must undoubtedly be minor, as greater than 97% of the variation in BSE graylevels can be accounted for by mineral content alone.

It is illustrative to compare BSE technology with the more traditional measurement of microscopic mineralization, microradiography. The resolution of BSE is unquestionably superior[23,35] as can be clearly observed in comparative images (**Figure 3**). The present study clearly demonstrates the strength of the correlation between BSE graylevels and mineral content. Previous studies have quantified the consistency of repeated measurements.[5,44] The present investigators are unaware of similar detailed studies of the accuracy, precision, and reproducibility of microradiographs. Additionally, BSE imaging does not require that all specimens be ground or milled to uniform thickness, thus greatly reducing specimen preparation time. Image capture is performed "on-line" allowing the investigator to rapidly visualize regions of interest and obtain images accordingly. Image capture takes approximately 10 sec, which is far less than the 30–45 min it takes to obtain a microradiograph. Collection of the approximately 100 images obtained in the present study, including calibration, took less than 4 h. Furthermore, because all images are digitally collected and stored on magnetic media for future analysis, the development of photographic films is not required. This eliminates the need for cumbersome video digitization and nonlinear calibration routines[28,29] for quantitative analysis of microradiographs.

The relative ease of use and accuracy of BSE imaging make it an ideal technique for investigating microscopic mineral variations. Large-scale studies involving numerous specimens, which were previously more technically difficult with the use of microradiographic techniques, can be examined more efficiently. Potential applications of this technology include both basic bone

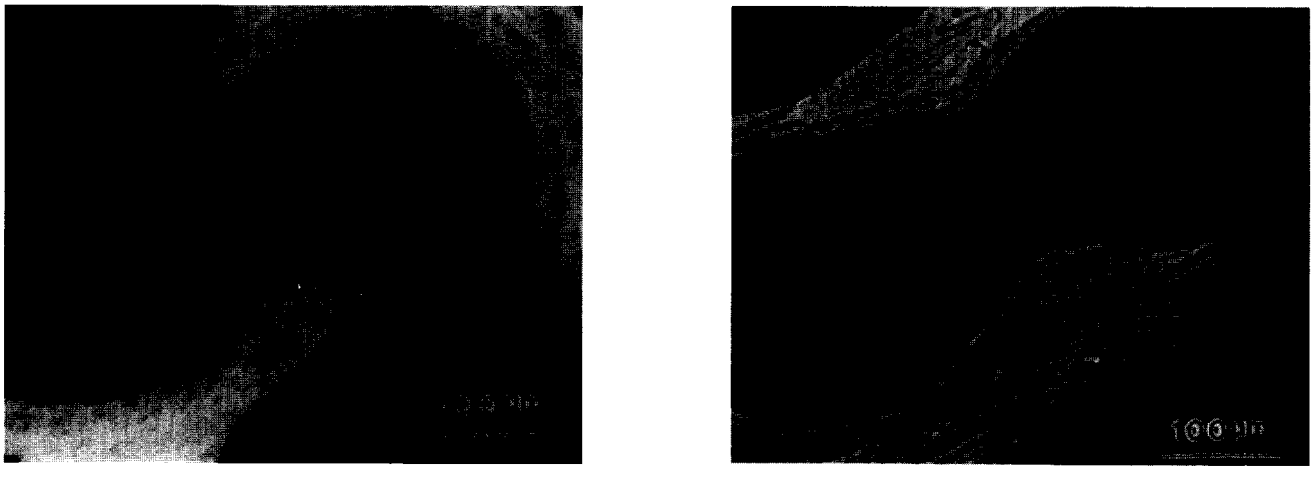

Figure 3. (a) Microradiograph taken from the vertebral body of a 3-year-old male beagle dog. The specimen was ground to a thickness of 100 μm and imaged with a custom-made microradiograph unit, using high-resolution spectroscopic plates. (b) BSE photomicrograph obtained from the same region as (a). Resolution of morphological features is superior in the BSE image. Similarly, enhanced graylevel discrimination can be observed in the BSE image.

Bone Vol. 20, No. 5
May 1997:485–490

research, clinical histometry, and mineral content analysis. The study of pathological mineralization, aging influences, the development of animal models for mineralization studies, and responses to treatment therapies should benefit from the further application of quantitative BSE imaging to bone.

Acknowledgments: The authors acknowledge the Department of Veterans Affairs Medical Research Fund, Salt Lake City, UT, for their support of this project; Gwenevere Shaw for her assistance in manuscript preparation; Dr. Frank Whitmore (Smithsonian Institute), Dr. Dennis M. Bramble (University of Utah), and the Los Angeles County Museum of Natural History for the donation of bone specimens; Norian Corporation for assistance in FTIR and XRD specimen analyses; and Dr. Scott C. Miller for his assistance obtaining microradiographs.

References

1. Amprino, R. and Engstrom, A. Studies on x-ray absorption and diffraction of bone tissue. Acta Anat 15:1–22; 1952.
2. Bachus, K. N. and Bloebaum, R. D. Projection effect errors in biomaterials and bone research. Cells Mater 2:347–355; 1992.
3. Biltz, R. M. and Pellegrino, E. D. The chemical anatomy of bone. I. A comparative study of bone composition in sixteen vertebrates. J Bone Jt Surg [Am] 51-A:456–466; 1969.
4. Bloebaum, R. D., Bachus, K. N., and Boyce, T. M. Backscattered electron imaging: The role in calcified tissue and implant analysis. J Biomater Appl 5:56–85; 1990.
5. Boyce, T. M., Bloebaum, R. D., Bachus, K. N., and Skedros, J. G. Reproducible method for calibrating the backscattered electron signal for quantitative assessment of mineral content in bone. Scann Microsc 4:591–603; 1990.
6. Boyde, A., Elliott, J. C., and Jones, S. J. Stereology and histogram analysis of backscattered electron images: Age changes in bone. Bone 14:205–210; 1993.
7. Boyde, A. and Jones, S. J. Back-scattered electron imaging of skeletal tissues. Metab Bone Dis Rel Res 5:145–150; 1983.
8. Boyde, A. and Jones, S. J. Scanning electron microscopy of bone: Instrument, specimen, and issues. Microsc Res Technol 33:92–120; 1996.
9. Boyde, A., Jones, S. J., Aerssens, J., and Dequeker, J. Mineral density quantitation of the human cortical iliac crest by backscattered electron image analysis: Variations with age, sex, and degree of osteoarthritis. Bone 16:619–627; 1995.
10. Boyde, A., Maconnachie, E., Reid, S. A., Delling, G., and Mundy, G. R. Scanning electron microscopy in bone pathology: Review of methods, potential and applications. Scann Electron Microsc 4:1537–1554; 1986.
11. Cullity, B. D. Elements of X-Ray Diffraction. Reading, MA: Addison-Wesley; 1978; 99–106.
12. Currey, J. D. The mechanical consequences of variation in the mineral content of bone. J Biomech 2:1–11; 1969.
13. Currey, J. D. Mechanical properties of bone tissues with greatly differing functions. J Biomech 12:313–319; 1979.
14. Currey, J. D. The Mechanical Adaptations of Bones. Princeton, NJ: Princeton University Press; 1984; 88–97.
15. Currey, J. D. The effect of porosity and mineral content on the Young's modulus of elasticity of compact bone. J Biomech 21:131–139; 1988.
16. Driessens, F. and Verbeeck, R. The dynamics of bone mineral in some vertebrates. Z Naturforsch 41:468–471; 1986.
17. Emmanual, J., Hornbeck, C., and Bloebaum, R. D. A polymethyl methacrylate method for large specimens of mineralized bone with implants. Stain Technol 62:401–410; 1987.
18. Fratzl, P., Schreiber, S., Roschger, P., Lafage, M.-H., Rodan, G., and Klaushofer, K. Effects of sodium fluoride and alendronate on the bone mineral in minipigs: A small-angle X-ray scattering and backscattered electron imaging study. J Bone Miner Res 11:248–253; 1996.
19. Glimcher, M. J. The nature of the mineral component of bone and the mechanism of calcification, American Academy of Orthopedic Surgery, 62nd Annual Meeting (Instructional Course Lecture 105), 1995, 49–69.
20. Goldstein, J. I., Newbury, D. E., Echlin, P., Joy, D. C., Romig, A. D., Jr., Lyman, C. E., Fiori, C., and Lifshin, E. Scanning Electron Microscopy and X-ray Microanalysis. A Text for Biologists, Materials Scientists, and Geologists. New York: Plenum; 1992; 417–436.
21. Grynpas, M. D. and Holmyard, D. Changes in quality of bone mineral on aging and in disease. Scann Microsc 2:1045–1054; 1988.
22. Heinrich, K. F. J. Electron probe microanalysis by specimen current measurement. Proceedings of the Fourth International Congress on X-Ray Optics and Microanalysis. Paris: Hermann; 1966; 159–167.
23. Howell, P. G. T. and Boyde, A. Monte Carlo simulations of electron scattering in bone. Bone 15:285–291; 1994.
24. LeGeros, R. Z. Apatites in biological systems. Prog Cryst Growth Charact 4:1–45; 1981.
25. Lloyd, G. E. Atomic number and crystallographic contrast images with the SEM: A review of backscattered electron techniques. Mineralogical Magazine 51:3–19; 1987.
26. Lowenstam, H. and Weiner, S. On Biomineralization. New York: Oxford; 1989; 151.
27. Martin, R. B. and Burr, D. B. Structure, Function and Adaptation of Compact Bone. New York: Raven; 1989; 80–81.
28. Martin, R. B., Papamichos, T., and Dannucci, G. A. Linear calibration of radiographic mineral density using video-digitizing methods. Calcif Tissue Int 47:82–91; 1990.
29. McQueen, C. M., Smith, D. A., Monk, I. B., and Horton, P. W. A television scanning system for the measurement of the spatial variation of micro-density in bone sections. Calcif Tissue Res 11:124–132; 1973.
30. Pechak, D. G., Kujawa, M. J., and Caplan, A. I. Morphology of bone development and bone remodeling in embryonic chick limbs. Bone 7:459–472; 1986.
31. Reid, S. A. and Boyde, A. Changes in the mineral density distribution in human bone with age: Image analysis using backscattered electrons in the SEM. J Bone Miner Res 2:13–22; 1987.
32. Richelle, L. J. and Onkelinx, C. Recent advances in the physical biology of bone and other hard tissues. In: Comar, C. and Bronner, F., Eds. Mineral Metabolism: An Advanced Treatise. New York: Academic; 1969; 123–190.
33. Roschger, P., Plenk, H., Jr., Klaushofer, K., and Eschberger, J. A new scanning electron microscopy approach to the quantification of bone mineral distribution: Backscattered electron image grey-levels correlated to calcium Kα-line intensities. Scann Microsc 9:75–88; 1995.
34. Roufosse, A., Landis, W., Sabine, W., and Glimcher, M. Identification of brushite in newly deposited bone mineral from embryonic chicks. J Ultrastruc Res 68:235–255; 1979.
35. Rowland, R., Jowsey, J., and Marshall, J. Microscopic metabolism of calcium in bone. III. Microradiographic measurements of mineral density. Radiat Res 10:234–242; 1959.
36. Sanderson, C. Polymerization of mineralized bone specimens embedded in methylmethacrylate using ultraviolet irradiation. J Histotechnol 18:323–325; 1995.
37. Sanderson, C. and Kitabayashi, L. R. Parallel experience of two different laboratories with the initiator perkadox 16 for polymerization of methylmethacrylates. J Histotechnol 17:343–348; 1994.
38. Skedros, J. G., Bloebaum, R. D., Bachus, K. N., and Boyce, T. M. The meaning of graylevels in backscattered electron images of bone. J Biomed Mater Res 27:47–56; 1993.
39. Skedros, J. G., Bloebaum, R. D., Bachus, K. N., Boyce, T. M., and Constantz, B. Influence of mineral content and composition on graylevels in backscattered electron images of bone. J Biomed Mater Res 27:57–64; 1993.
40. Skedros, J. G., Mason, M. W., Nelson, M. C., and Bloebaum, R. D. Evidence of structural and material adaptation to specific strain features in cortical bone. Anat Rec 246:47–63; 1996.
41. Squillante, R. G. and Williams, J. L. Videodensitometry of osteons in females with femoral neck fractures. Calcif Tissue Int 52:273–277; 1993.
42. Sumner, D. R., Bryan, J. M., Urban, R. M., and Kuszak, J. R. Measuring the volume fraction of bone ingrowth: A comparison of three techniques. J Orthop Res 8:448–452; 1990.
43. Torontali, M., Koo, I., Holmyard, D. P., Tomlinson, G., Grynpas, M. D., and Tenenbraum, H. C. Backscattered electron image assessment of mineral density in bone formed *in vitro*. Cells Mater 4:125–134; 1994.
44. Vajda, E. G., Skedros, J. G., and Bloebaum, R. D. Consistency in calibrated backscattered electron images of calcified tissues and mineral analyzed in multiple imaging sessions. Scann Microsc 9:741–755; 1995.
45. Zou, L., Bloebaum, R. D., and Bachus, K. N. Reproducibility of techniques using Archimedes' principle in measuring cancellous bone volume. Med Eng Phys. In press.

Date Received: December 26, 1996
Date Accepted: January 30, 1997